Coagulation and Adhesion of Nanoparticles generated in flame from droplets of Nickel Nitrate aqueous solutions

F. Carbone[1], A. C. Barone[2], A. De Filippo[1], F. Beretta[3], A. D'Anna[1], A. D'Alessio[1]

[1]Dipartimento di Ingegneria Chimica – Università degli Studi di Napoli 'Federico II'
Piazzale Tecchio 80, 80125 Napoli, Italy
[2]Istituto Italiano di Tecnologia (IIT)
Via Morego 30, 16163 Genova, Italy
[3]Istituto di Ricerche sulla Combustione – CNR
Piazzale Tecchio 80, 80125 Napoli, Italy

Ashes and additives present in practical fuels, biomass and wastes contain a not negligible amount of metals which brought at high temperature, cause the emission of ultrafine particles. In this paper we generate nickel oxides nanoparticles smaller than 5nm by quickly heating droplets of Nickel(II) Nitrate aqueous solutions in two different flame reactors. Nanoparticles sizing was performed using complementary diagnostics: Atomic Force Microscopy (AFM) and Differential Mobility Analysis (DMA). We show that nanoparticles smaller than 5nm are easily produced in these flame reactors and exhibit coagulation rate orders of magnitude lower than the gas kinetic collision rate. Furthermore extra-situ AFM measurements demonstrate that also the adhesion efficiency behaves similar to coagulation becoming extremely small for size smaller than 3nm. These results imply that smallest metal nanoparticles produced during combustion may be easily dispersed into the atmosphere because they have a much longer life-time than generally assumed and may easily bounce on surfaces or filters.

1. Introduction

It is well known that metals present as ashes or additives into the fuels, brought at high temperature in combustion devices, generate a large range of particulate which extend in the ultrafine range (Linak and Wendt, 1993). The formation of nanosized particles is also reasonable because the addition of metal precursors in flames is a widely diffused technique used to produce nanopowders (Pratsinis, 1998). Up to recent times the nanometric fraction, i.e. below 5nm, was not taken in consideration because of two reasons. Firstly the commercial diagnostics were able to detect only particles larger than 5nm. On the other hand it was assumed that such small particles meet and coagulate at gas kinetic rate so that their lifetime was negligible small (Hinds, 1999).
Recent advances in diagnostics, either with Atomic Force Microscopy (AFM) or with Differential Mobility Analysis (DMA), have extended the field of measurability for nanoparticles in flame down to 1nm (D'Alessio et. al., 2005, Sgro et al., 2007). On these bases it was realized that coagulation rate of carbonaceous nanoparticles at high temperature, as well their adhesion rate, drops dramatically orders of magnitude as their size decreases below 3nm. Consequently those nanoparticles may escape from combustors and survive in the atmosphere in a not negligible amount. The emission of

such small nanoparticles could involve a severe pollution problem since recent toxicological results have shown that particle toxicity increases with decreasing size and depends on number density (Oberdorster et al., 2005).

The main purpose of this communication is to discover if the production of extremely small nanoparticles take place when metals are introduced in combustion systems and whether their coagulation and adhesion rate, at high temperature, follow the same trend of carbonaceous nanoparticles. To this purpose we designed two laboratory experiments that allow studying the nanoparticles behavior at different temperatures. In both experiments, nickel oxides nanoparticles were generated by heating droplets of Nickel(II) Nitrate, $Ni(NO_3)_2$, aqueous solutions in flames. The flame provides the environment for droplets fast heating and transformation to particles. Nickel was preferred to other pollutant metals because its oxides, generated by $Ni(NO_3)_2$ thermal decomposition (Brockner et al., 2007), are not volatile at flames temperature (Linak and Wendt, 1993). Therefore the absence of vapor phase avoids particles surface growth and simplifies results interpretation because nanoparticles, once generated, are only able to coagulate.

Particles were thermophoretically collected on mica substrates for AFM dimensional analysis. AFM, producing three-dimensional image of the samples, allows to measure objects volume preventing size evaluation errors of not spherical particles caused by bi-dimensional imaging of other microscopy techniques (Barone et al., 2003). On-line size distributions measurements by high resolution DMA was also performed on one reactor. The nanoparticles dynamic was investigated by performing measurements at several heights above the burner (HAB) or, equivalently residence times (RT), in flame. The observed coagulation rate is compared to the Brownian collision rate to evaluate the nanoparticles coagulation efficiency. The amount and sizes of particles collected on substrates for AFM analysis was compared to that impinging on its surface by thermophoresis in order to evaluate the adhesion/collection efficiency depending on particle diameter.

2. Experimental

Two laboratory reactors, simulating combustion conditions and generating metal nanoparticles, were experimentally investigated. Both reactors consist of a laminar premixed flame doped with droplets of $Ni(NO_3)_2$ aqueous solutions. The monodisperse solution droplets, fed in both reactors, are generated by a Berglund-Liu-type Vibrating Orifice Aerosol Generator (model 3450, TSI).

The first investigated reactor is a stoichiomentric flat laminar premixed flame of ethylene/air (cold gas flow velocity of 80mm/s) stabilized on a water cooled brass porous-plug McKenna-type burner. The porous-plug was drilled on its axis where a 7.5mm ID stainless-steel tube is inserted to carry into the flame core an air dispersion (flow rate of 600cm^3/min) of 40μm $Ni(NO_3)_2$ solution (mass concentration of 25%) droplets. The fed solution flow rate is 0.139cm^3/min. The addition of the solution droplets involves the appearance of a light emitting jet (fig.1a) whose flicker is reduced placing a flat plate at 40mm of height above the burner (HAB). This reactor presents radial unhomogeneity but we just perform nanoparticles measurements on the flame axis, where metal precursor is axially fed. Nanoparticles dynamic at increasing RT up

till 12ms was investigated performing the measurements at several HAB up to HAB=35mm. An expected aerosol volume fraction (fv_{Ex}), constant along flame axis, is calculated by a material balance of fed metal. The balance was performed assuming the particles density equal to that of bulk Nickel(II) Oxide (NiO) or Nickel (Ni). We obtain 1ppm and 0.56ppm, respectively. The main approximation is that the metal disperses into 5% of hot gas stream. The value calculated by this balance using $Pb(NO_3)_2$ instead of $Ni(NO_3)_2$ solution was reported to agree with that in-situ measured by light extinction (Carbone et al., 2008).

The second reactor is a fuel lean laminar premixed flame (cold gas velocity 300mm/s) of methane/oxygen/nitrogen in the ratios 1/2.6/8, homogeneously doped with metal precursor droplets. The flame (fig.1b) was stabilized on a properly designed burner similar to that used by Arabi-Katbi et al. (2002). The burner consist of a 40mm long Mullite Zirconia honeycomb (400CPSI, CTI s.a.) placed on the top of a 18mm ID stainless-steel tube. The honeycomb both stabilizes the flame and it allows the homogeneous addition of the particles precursor droplets. Another stainless steel tube, coaxial to the burner, provides an outside ring (ID 24 mm and OD 32 mm) used for flowing the sheath N_2 (flow rate of 3400 cm³/min) to minimize the entrainment of the surrounding air. We disperse 0.089 cm³/min of 25μm $Ni(NO_3)_2$ aqueous solution (mass concentration 4%) droplets into the cold gas mixture. The obtained premixed flame may be assumed as a plug flow reactor. Performing measurements at several HAB (up to 50mm), this experimental configuration allows investigating longer nanoparticles RT (~26ms) with respect to McKenna-type burner.

We measures temperature along the flames axis using a 125μm Pt/Pt-13%Rh thermocouple (Type R, Omega Engineering) and substituting the solution with bidistilled water to prevent nanoparticles deposition on the measurement junction. Measured temperature was corrected for radiative lost. For the McKenna-type burner temperature increases from the droplets injection point to HAB=20mm where nascent nanoparticles were measured and droplets fully evaporated during about 20ms. At higher HAB, temperature remains almost constant around ~1200K (Carbone et al., 2008). For the honeycomb burner, temperature increases up to ~2050K from the burner surface to just downstream the flame front, then it slowly decreases (~1600K at HAB=50mm). Droplets fully evaporated during less than 2.5ms, upstream HAB=5mm where we early measure incipient nanoparticles. Post flame axial temperature profiles of both reactors are reported versus RT in fig.1c. The zero RT was assumed at the lowest HAB where nanoparticles measurements were performed (20mm and 5mm for McKenna-type and Honeycomb burners, respectively).
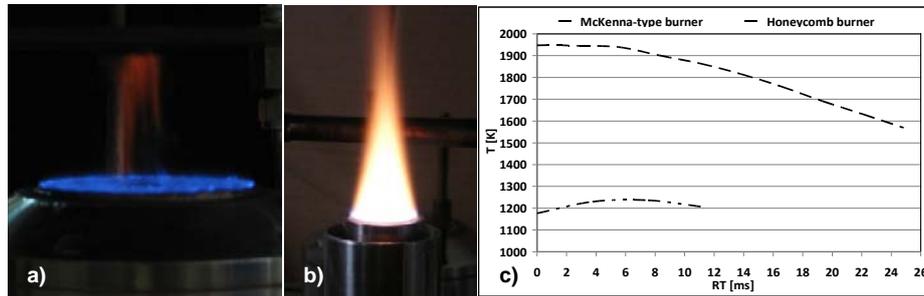
Fig.1 a) McKenna burner; b) Honeycomb burner; c) temperature profiles.

2.1 Atomic Force Microscopy

Particles are thermophoretically collected on mica muscovite disks (3mm diameter) inserted parallel to the gas streamline using a properly designed pneumatic actuator that assures a quick insertion and a constant sampling time ($\Delta t \sim 30ms$). An Atomic Force Microscope (Nanoscope IIIa™, Digital Instruments), operating in tapping-mode, generates a topological three-dimensional image of the samples (Barone et. al., 2003). Advanced image processing (S.P.I.P.™, ImageMetrology) is performed to obtain volumes of collected particles. Particles equivalent diameter (ED) is calculated as the diameter of a sphere having the measured particle volume. Results are converted in ED normalized frequency distribution subsequently fitted by a weighted sum of lognormal distributions allowing its easy handling. AFM analysis estimates also the aerosol volume fraction (fv) or number concentration (N) in order to obtain absolute ED distributions. Since the generated particles are within the free molecular regime, the particles thermophoretic velocity does not depend on particles size ($V_{th}=0.55\nu\nabla T/T$) and it only depends on the thermal laminar boundary layer thickness (δ_{th}) above mica surface (Hinds, 1999). Indeed $\nabla T=(T_{gas}-T_{mica})/\delta_{th}$ is the temperature gradient between the gas and the substrate ($T_{mica}\sim350K$), ν is the gas kinematic viscosity and T is the particles absolute temperature ($T\sim(T_{mica}+T_{gas})/2$). The product of the imaged surface (usually $S_{im}=4\mu m^2$), thermophoretic velocity and sampling time gives the aerosol sampled volume ($Vol_{sam}=S_{im}V_{th}\Delta t$). The collected particles total volume or number to gas sampled volume ratios are $fv_{AFM}=Vol_{part}/Vol_{sam}$ and $N_{AFM}=N_{part}/Vol_{sam}$, respectively. These values agree with real fv and N only if each particle, impinging on the substrate, bonds on the substrate. Low value of adhesion/collection efficiency conducts AFM to underestimate fv and N. Furthermore, size dependent adhesion efficiency affects the shape of AFM measured size distribution overestimating the frequency of more effectively collected particles.

2.2 Differential Mobility Analysis

Mobility Diameter (MD) distributions of nanoparticles produced with the honeycomb burner are on-line measured using a dilution probe and a TapCon 3/150 DMA system (nominal MD range 0.6–28 nm) equipped with a Faraday Cup Electrometer detector (Sgro et al., 2007). MD is slightly larger than ED in the size range smaller than 3 nm because of an effective diameter ($D_0= 0.5$ nm for air) of particles-free gas sheath in the

electrostatic classifier (Fernandez de la Mora, 2003) implying ED=MD- D_0. We report results in term of ED distributions and obtained using this relation. Following published work, we used a horizontal tube rapid dilution probe (8mm ID, 0.5mm wall thickness, 0.3 mm orifice diameter) to transport and cool sampled aerosol (Kasper et al., 1997). Earlier work examining dilution probes found that particle coagulation in the probe may significantly change the shape of the size distribution (Kasper et al. 1997, Zhao et al., 2003). Experimentally, particle coagulation is suppressed by varying the dilution ratio in order to attain a critical value. Above this value the size distribution does not change and the eventual changing of particles number is inverse proportional to the dilution itself. The dilution ratio was controlled by monitoring a slight underpressure in the probe, manually controlled with a rotary vane vacuum pump, while holding the particle free dilution N_2 flow constant at 29 lpm. The sample flow rate was calibrated by measuring CO_2 concentrations with a non-dispersive infrared analyzer (Hartmann & Braun URAS 10E) drawn in from flames with the probe operating exactly as it was during particle size distribution measurements (Zhao et al., 2003).

3. Results and discussions

3.1 McKenna-type burner

AFM image processing recognizes from 160 to 320particles/μm^2 on the substrate, depending on the sampling HAB. The distributions are shown in fig.2a; points are normalized frequency and lines their best fittings. A bimodal nature is observed from the beginning while particles are monodisperse at longer RD. At HAB=20mm (RD=0ms) the size distribution is characterized by first mode mean ED (MED) and standard deviation (SD) of 3.4nm and 0.9nm, respectively. The second mode particles have 12nm MED and 5nm SD, representing 4% of total collected particles number. After RD~3.7ms (HAB=25mm) first mode MED (3.1nm) and SD (0.8nm) are slightly smaller while the second mode particles (jet 4% of total number) shrink significantly (9.7nm MED and 4.1nm SD). After RD~7.5ms (HAB=30mm) the first mode still have 3.3nm MED and 0.8nm SD while the second mode, subjected to a further shrink (5.6nm MED and 1.4nm SD), is collapsing into the first mode. The latter completely disappears at HAB=35mm (RD~11.3ms) where almost monodisperse particles (4.2nm MD and 1nm SD) are sampled.
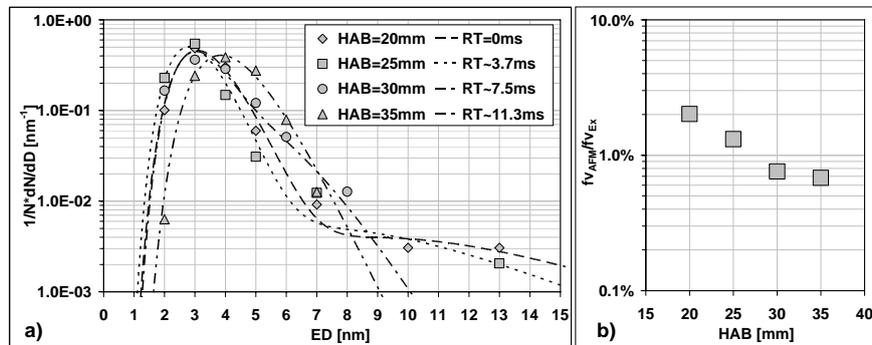

Fig.2 McKenna burner: a) AFM ED normalized distributions; b) Adhesion efficiency.

We calculate $N \sim 4.5 \times 10^{13} cm^{-3}$ of monodisperse ED~3nm particles from the $fv_{Ex}(NiO)$. AFM measurements show ~10ms half-life of those first mode particles. This value is about three orders of magnitude longer than the gas kinetic half-life (~35μs) calculated, at the obtained N and T, assuming each collision, due to thermal motion, involves coagulation (Hinds, 1999). The nanoparticles lifetime longer than expected involves a coagulation efficiency of $\sim 10^{-3}$ for ED~3nm while value close to unity are commonly reported for larger particles. Thus there is a size dependent coagulation efficiency quickly decreasing with decreasing ED below 5nm. The nanoparticles adhesion efficiency is investigated by the fv_{AFM} to $fv_{Ex}(NiO)$ ratio axial profile (Fig.2b). This ratio represents the mean value of particles collection/adhesion efficiency and it always attains value about two orders of magnitude lower than unity. Mean adhesion efficiency decreases from ~2% to ~0.7% simultaneously disappearing of larger particles downstream into the flame. Thus there is size dependent adhesion efficiency quickly decreasing for ED<5nm, similarly to coagulation efficiency. It reach value about two orders of magnitude lower than unity for the monodisperse ~4nm particles detected at HAB=35mm. The normalized frequency of aerosol particles with ED below 5nm could be much higher than that measured on the substrate while MED is probably lower than that measured by AFM because of the lowering of collection efficiency with decreasing nanoparticles size below 5nm (D'Alessio et al., 2005).

3.2 Honeycomb Burner
On-line aerosol measurements were performed by DMA at several HAB. Some representative measured distributions are reported in fig.3a. They always show a sub-nanometer peak detected also in particles free gasses and probably due to formation of molecular clusters during ionization process (Sgro et al., 2007). This sub-nanometer peak also gives a negligible contribution to fv calculation, thus is not considered to represent particles and it is not further discussed in this paper. The particles distributions show a behavior quite similar to that observed for the McKenna-type burner. Indeed it is bimodal at HAB=5mm while particles are monodisperse at longer RD. At HAB=5mm (RD=0ms) first mode MED and SD are 2.8nm and 1.2nm, respectively while second mode, about 0.1% of total particles number, have 13nm MED and 3.2nm SD. Particles larger than 10nm quickly disappear after RD~1.4ms (at HAB=7.5mm) and almost the same monomodal distribution (2.7nm-2.9nm MED and 1nm-1.3nm SD) is measured up to HAB=50mm (RD~25ms). We also report in fig.3a two distributions measured at HAB=15mm at the beginning (I) and at the end (II) of the experiment. They show a negligible loss of particles (1%), expecially for larger ED, due to a slight clogging of probing pinhole after about 2 hours of measurements and they also indicate measurements uncertainty.

Integrating the measured distributions, we calculate almost constant fv~0.22ppm and $N \sim 1.2 \times 10^{13} cm^{-3}$ axial profiles. Thus it is evident that, once generated, the ED~2.8nm particles do not coagulate in spite gas kinetic theory implies, at the measured N and T, a half-life of about 150μs for those Brownian particles (Hinds, 1999). The unchanging of distribution during the investigated RD~25ms, involves values of coagulation efficiency at least tree orders of magnitude lower than unity for ED~2.8nm.
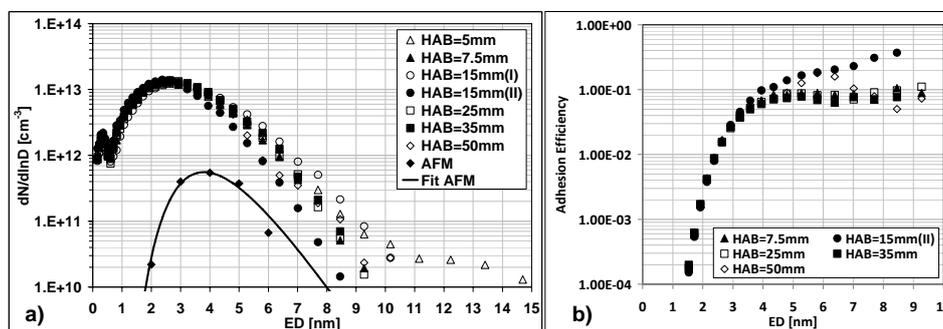
Fig.3 Honeycomb burner: a) ED distributions; b) Adhesion efficiency.

We also collected 500-600particles/μm^2 on mica substrates at several HAB to perform their AFM image analysis. Roughly the same monomodal aerosol distribution was obtained at all HAB. That distribution obtained at HAB=15mm is also reported in fig.3a.It is representative of distribution at each HAB and has MED=3.9nm and SD=1nm. Points represent ED absolute frequency and the line is the best fitting. Almost constant value of $N_{AFM} \sim 3.5*10^{11} cm^{-3}$ and $fv_{AFM} \sim 10ppb$ were calculated. Then also AFM results show the not coagulating behavior of those nanoparticles with size lower than 5nm. Furthermore N_{AFM} and fv_{AFM} values are much lower then that on-line measured by DMA because the mean adhesion efficiency is about two orders of magnitude lower than unity. Comparison of AFM with DMA distributions shows that the larger amounts of uncollected particles are those with lowest ED because of size dependent collection efficiency. The ED dependence of adhesion efficiency was obtained by the AFM to DMA distributions ratio and is showed in fig.3b. It quickly decreases for ED lower than 5nm reaching values about two orders of magnitude lower than unity for ED~2.5nm. This behavior, quite similar to that observed for carbonaceous nanoparticles (D'alessio et al., 2005), conducts AFM to overestimate the real MED.

3.2 Comparative discussions

Results obtained on the two different reactors are quite similar in spite of different temperature values. The formation of such small nanoparticles seems to be related more on droplets heating rate than on temperature itself. A vapor phase nanoparticles formation pathway is to be excluded also because NiO and Ni are not volatile at the measured temperatures (Linak and Wendt, 1993). We speculate that nanoparticles nucleation occurs inside the droplets, as already proposed in literature (Limaye and Helble, 2002). The nuclei are released into the gas before their aggregation, growth or diffusion inside the droplet can occur because of evaporation quickness. The smallest nuclei are almost instantaneously heated and decomposed (573K) (Brockner et al., 2007) to NiO ~2.5nm particles while larger ones decomposition requires longer time because of their lower specific surface area slowing nitrides release. The nanoparticles loss of mass, involved during this decomposition, is compatible with the measured second mode shrinking observed in both experiment and it is faster for Honeycomb burner because of its higher temperature. Furthermore particles larger than 10nm measured by DMA at HAB=5mm of the Honeycomb burner are not detected by AFM

measurements. This may be an effect of flame cooling by DMA dilution probe slowing the nitrate decomposition.

4. Conclusion

We generate nickel oxides nanoparticles of few nanometers in a wide range of high temperatures. Particles sizing is performed with two diagnostics and all the results are in quite good agreement. They show a lifetime of particles with size below 5nm, much longer then expected by gas kinetic theory implying that coagulation efficiency is orders of magnitude lower than unity. The amount of particles collected on substrates for AFM analysis was always lower than that impinging on its surface by thermophoresis. Moreover collected particles sizes are slightly larger than those measured on-line by DMA. Then the particles adhesion/collection efficiency strongly depends on particle size and decreases of orders of magnitude with decreasing diameter below 5nm. This behavior is in agreement with the results obtained for carbonaceous nanoparticles (D'Alessio et al., 2005). Metal nanoparticles with size smaller than 5nm could, therefore, potentially survive exhaust conditions and filtering devices because of their low coagulation and adhesion efficiency, not negligibly contributing to air pollution.

5. References

Arabi-Katbi, O.I., Wegner, K. and Pratsinis, S.E., 2002, Ann. Chim. Sci. Mat. 27(6), 37.

Barone, A.C., D'Alessio, A. and D'Anna, A., 2003, Combust. Flame 132,181.

Brockner, W., Ehrhardt, C. and Gjikaj, M., 2007 Thermochimica Acta 456, 64.

Carbone, F., Barone, A.C., Pagliara, R., Beretta, F., D'Anna, A. and D'Alessio, A., 2008, Environ. Eng. Sci. in press.

D'Alessio, A., Barone, A.C., Cau, R., D'Anna, A. and Minutolo, P., 2005, Proc. Combust. Inst. 30, 2595.

Fernadez de la Mora, J.J., De Juan, L.L., Liedtke, K. and Schmidt-Ott, A., 2003, J. of Aeros. Sci. 34, 79.

Hinds, W. C.,1999, Aerosol Technology. John Wiley & Son, New York.

Kasper, M., Siegmann, K. and Sattler, K., 1997, J. Aerosol Sci. 28, 1569.

Limaye, A.U. and Helble, J.J., 2002, J. Am. Ceram. Soc. 85, 1127.

Linak, W.P. and Wendt, J.O.L., 1993, Prog. Energy Combust. Sci. 19, 145.

Oberdorster, G., Oberdorster, E. and Oberdorster, J., 2005, J. Environ. Health Perspectives 113, 823.

Pratsinis, S.E.,1998, Prog. Energy Combust. Sci. 19, 145.

Sgro, L.A., De Filippo, A., Lanzuolo G. and D'Alessio, A., 2007, Proc. Combust. Inst. 31, 631.

Zhao, B., Yang, Z., Wang, J., Johnston, M.V. and Wang, H., 2003, Aerosol Sci. Technol. 37, 611